Contents lists available at ScienceDirect

Journal of Inorganic Biochemistry

journal homepage: www.elsevier.com/locate/jinorgbio

Tuning the Mn_2^{II}/Mn_2^{III} redox cycle of a phenoxo-bridged diMn catalase mimic with terminal carboxylate donors

Verónica Solís[a], Claudia Palopoli[a], Verónica Daier[a], Eric Rivière[b], Fabrice Collin[c,d,e], Diego M. Moreno[a], Christelle Hureau[c,d], Sandra Signorella[a,*]

[a] IQUIR (Instituto de Química Rosario), Consejo Nacional de Investigaciones Científicas y Técnicas (CONICET), Facultad de Ciencias Bioquímicas y Farmacéuticas, Universidad Nacional de Rosario, Suipacha 531, S2002LRK Rosario, Argentina
[b] Institut de Chimie Moléculaire et des Matériaux d'Orsay, CNRS, Université Paris Sud, Université Paris Saclay, 91405 Orsay Cedex, France
[c] UPS, INPT, Université de Toulouse, 205 route de Narbonne, F-31077 Toulouse, France
[d] CNRS, LCC (Laboratoire de Chimie de Coordination), France
[e] UMR 152 Pharma Dev, Université de Toulouse, IRD, UPS, France

ARTICLE INFO

Keywords:
Catalase mimic
Manganese
Kinetics
Polycarboxylate ligand

ABSTRACT

A new phenoxo-bridged $diMn^{III}$ complex, $Na[Mn_2L(OH)_2(H_2O)_2]\cdot 5H_2O$ (**1**), obtained with the ligand L^{5-} = 5-methyl-2-hydroxo-1,3-xylene-α,α-diamine-*N,N,N′,N′*-tetraacetato, has been prepared and characterized. Mass spectrometry, conductivity, UV–visible, EPR and ^1H NMR spectroscopic studies showed that the complex exists in solution as a monoanionic $diMn^{III}$ complex. Complex **1** catalyzes H_2O_2 disproportionation with second-order rate constant k_{cat} = 305(9) M^{-1} min^{-1} and without a time-lag phase. Based on spectroscopic results, the catalase activity of complex **1** in methanol involves a Mn_2^{III}/Mn_2^{II} redox cycle, which distinguishes this catalyst from other phenoxo-bridged diMn complexes that cycle between $Mn^{II}Mn^{III}/Mn^{III}Mn^{IV}$ species. Addition of base stabilizes the catalyst, restrains demetallation during catalysis and causes moderate enhancement of catalase activity. The terminal carboxylate donors of **1** not only contribute as internal bases to assist deprotonation of H_2O_2 but also favor the formation of active homovalent diMn species, just as observed for the enzyme.

1. Introduction

Manganese catalases (MnCAT) catalyze the disproportionation of harmful H_2O_2 into H_2O and O_2 by using a $Mn_2(\mu\text{-}O_2CR)(\mu\text{-}O/OH/H_2O)_2$ structural unit as the active site [1,2], with terminal carboxylates bound to the Mn ions to assist the proton transfer during catalysis [3]. The highly efficient dismutation of H_2O_2 by MnCAT requires a two-electron redox cycle that involves Mn_2^{II} and Mn_2^{III} oxidation levels [4,5]. When using artificial compounds to model the enzymatic activity, the fine-tuning of Mn redox states is a critical feature [6]. The number and type of ligands, the total charge, the nuclearity of the site, are among the factors that introduce a way of tuning the oxidation states of the metal center to face the redox reaction. Owing to their potential use as catalytic scavengers of H_2O_2 for preventing oxidative stress damage, many diMn complexes have been tested as MnCAT mimics [7,8]. Dinucleating ligands with a central alkoxo or phenoxo group afford a scaffold to enhance co-operativity between the two Mn ions and have been used to model the active site of MnCAT. While alkoxo-bridged diMn complexes decompose H_2O_2 through catalytic cycles involving homovalent Mn_2^{II}/Mn_2^{III} or Mn_2^{III}/Mn_2^{IV} active species [6–8], phenoxo-bridged diMn complexes of heptadentate ligands tested to date, employ mixed valence diMn species during catalysis [7,9–11]. $Mn^{II}Mn^{III}/Mn^{III}Mn^{IV}$ oxidations states were detected during disproportionation of H_2O_2 by phenoxo-bridged diMn complexes of ligands bearing terminal pyridyl [10], pyridyl/benzyl [9] and pyridyl/carboxylate [10] groups, instead of Mn_2^{II}/Mn_2^{III} states employed by the biosite. With the aim of determining the effect of replacing all terminal pyridyl by carboxylato donors on the active oxidation states of phenoxo-bridged diMn CAT mimics, we report here the synthesis, characterization and CAT activity, of a diMn complex with an *O*-rich coordination sphere $Na[Mn_2L(OH)_2(H_2O)_2]\cdot 5H_2O$ (**1**·$5H_2O$), obtained with the N_2O_5-ligand L^{5-} = 5-methyl-2-hydroxo-1,3-xylene-α,α-diamine-*N,N,N′,N′*-tetraacetato, and compare its catalytic activity with other phenoxo-bridged diMn models. Besides, we show that addition of an exogenous base stabilizes the catalyst and has moderate effect on the CAT activity thus confirming the role played by terminal carboxylato donors to assist proton transfer during H_2O_2 dismutation.

* Corresponding author.
E-mail address: signorella@iquir-conicet.gov.ar (S. Signorella).

https://doi.org/10.1016/j.jinorgbio.2018.01.013
Received 24 October 2017; Available online xxxx

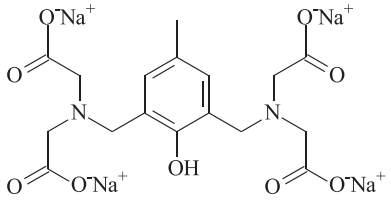

Na_4HL

2. Experimental section

2.1. Materials

All reagents or AR chemicals were used as purchased. Solvents were purified by standard methods. The concentration of H_2O_2 stock solution was determined by iodometric titration.

2.2. Synthesis of ligand and complex

2.2.1. Tetra sodium salt of 5-methyl-2-hydroxy-1,3-xylene-α,α-diamine-N,N,N′,N′-tetraacetic acid (Na_4HL)

The Na_4HL ligand was synthesized by a modification of the procedure of Schwarzenbach [12,13]. To a mixture of a 6.5 mL aqueous solution of 836.4 mg (6.28 mmol) of iminodiacetic acid and 2 mL aqueous solution of 346.8 mg (3.2 mmol) of *p*-cresol cooled in an ice-water bath were added 2 mL of 6.25 M NaOH. Upon dissolution, 0.75 mL of 37% formaldehyde was added dropwise. The solution was stirred for 30 min at 0 °C, heated at reflux for 5 h, and then concentrated to dryness. The solid was recrystallized from a 2:1 methanol:ethanol mixture. Colorless crystals of Na_4HL were filtered off, washed with ether and dried under vacuum. Yield: 1.3078 g (86%). ^{1}H NMR in D_2O, δ (ppm): 2.14 (s, 3H), 3.10 (s, 8H, N-$\underline{CH_2}$-CO_2); 3.65 (s, 4H, Ar-$\underline{CH_2}$-N), 6.91 (s, 2H, $\underline{H}_{Ar}$). ^{13}C NMR in D_2O, δ (ppm): 19.30 (Me); 55.03 (Ar-$\underline{C}$-N); 57.95 (N-$\underline{C}$-CO_2); 123.15 (C1/C3); 128.60 (C5); 131.38 (C4/C6); 158.10 ($\underline{C}_{Ar}$-OH); 179.00 ($\underline{C}O_2^-$). IR (KBr, ν cm^{-1}): 3422, 2923, 2826, 1594, 1481, 1411, 1328, 861, 725. $\underline{Mp}$: 270–271 °C. UV–vis, $\lambda_{máx}$ nm (ε M^{-1} cm^{-1}) in H_2O: 289 (3900), 315 (sh); in methanol: 290 (2140).

2.2.2. $Na[Mn_2L(OH)_2(H_2O)_2]\cdot 5H_2O$ (**1**$\cdot 5H_2O$)

To a solution of 52 mg (0.1069 mmol) of Na_4HL in 2.5 mL MeOH and 0.15 mL distilled H_2O, were added 75 μL (0.5372 mmol) of Et_3N and then a solution of 80.5 mg (0,2224 mmol) Mn $(ClO_4)_2\cdot 6H_2O$ in 1 mL H_2O. The reaction mixture was left with stirring during two days at room temperature. The solid was filtered off, and 20 mL of MeCN were added to the filtrate, after which the complex began to precipitate. The suspension was left one day without stirring and the solid decanted. The supernatant solution was separated and the solid was washed with ethyl ether and dried under vacuum. Yield: 34 mg (58.6%). Anal. calcd for $C_{17}H_{23}Mn_2N_2NaO_{13}\cdot 5H_2O$: C: 29.8, H 4.8, Mn 16.0, N 4.1%; Found: C 29.5; H 4.6; Mn 16.2; N 4.1%. UV–vis, $\lambda_{máx}$ nm (ε M^{-1} cm^{-1}) in MeOH: 239 (9962), 283 (6415), 380 (sh), 602 (190); in MeOH/Et_3N: 236 (17400), 276 (11630), 390 (5110). Significant IR bands (KBr, ν cm^{-1}): ν_{OH} 3425 (broad), $\nu_{C\text{-}H}$ 2922/2870,ν_{CO2-} 1602/1405, $\nu_{C\text{-}O/N}$ 1323, 1262. The content of five molecules of non-coordinated water per complex molecule was confirmed by thermogravimetric analysis of the complex which showed 13.5% mass loss below 150 °C. Molar conductivity = 96 Ω^{-1} cm^2 mol^{-1}.

2.3. Physical and analytical measurements

Electronic spectra were recorded on a JASCO V550 spectrophotometer with thermostated cell compartments. IR spectra were recorded on a Perkin-Elmer Spectrum One FT-IR spectrophotometer. Mass spectra were recorded on an ion trap mass spectrometer (ThermoScientific LCQ DECA XP Max) equipped with an electrospray ionization source (ESI-MS). The solutions for mass spectrometry were prepared from solutions of the complexes or reaction mixtures and diluted with methanol to a 100 μM concentration and directly infused at a flow rate of 10 μL min^{-1}. Melting point was taken on a Fisher-Johns (Ionomex) apparatus. ^{1}H and ^{13}C NMR spectra were recorded on a Bruker AC 300 NMR spectrometer at ambient probe temperature (ca. 26 °C). Paramagnetic NMR spectra were acquired using super WEFT sequence; with acquisition time of 67 ms. Magnetic susceptibility data were collected with a Quantum Design MPMS SQUID susceptometer. EPR spectra were obtained on a Bruker ESP 300 E spectrometer with a microwave frequency generated with a Bruker ER 04 (9–10 GHz). TGA measurements were conducted on a Perkin-Elmer Diamond TG/DTA Instrument. The compound was heated at the rate of 10 °C/min between RT and 1200 °C. Conductivity measurements were performed using a Horiba F-54 BW conductivity meter, on 1.0 mM solutions of the complexes in methanol. The Mn content was measured by atomic absorption on a METROLAB 250 AA spectrophotometer. The Na content was determined by atomic absorption on an UNICAM spectrophotometer, model 969, at 5890 Å. The electrochemical experiments were performed with a computer controlled Princeton Applied Research potentiostat, model VERSASTAT II, with model 270/250 Research Electrochemistry Software. Studies were carried out under Ar, in aqueous buffered solutions (50 mM Et_3N–Et_3NH^+, pH = 10) using 0.1 M $NaNO_3$ as supporting electrolyte and ~10^{-3} M of the complex. The working electrode was a Pt wire, and the reference electrode was Ag/AgCl with Pt as the auxiliary electrode. Potentials are referred to the Ag/AgCl/sat KCl electrode. Under these conditions, the reduction peak of the Zobell's solution was observed at 229 mV (vs Ag/AgCl/sat KCl).

2.4. Evaluation of CAT activity

Reaction rates were determined by volumetric measurement of the O_2 evolved after addition of excess of H_2O_2 to a solution of the complex. A round-bottom flask with a rubber septum, containing the degassed solution of the complex, was thermostated at 25 °C and connected to a gas-measuring burette (precision of 0.1 mL). Previously thermostated H_2O_2 was injected through the septum to the stirred complex solution, and the evolved O_2 was measured with the burette. The initial reaction rates were obtained by fitting the [O_2] versus time data to a polynomial expression [14] and calculating the slope of the tangent at time zero. Each rate constant reported here represents the mean value of multiple determinations that fall within ± 5%. All experiments were carried out at 25 °C. Blanc experiments performed with 125 mM H_2O_2 in 50 mM Et_3N without the catalyst showed that after 2 h only 2% of the initial H_2O_2 had disproportionated, while when the catalyst (0.5 mM) was present, all H_2O_2 decomposed in 20 min. When 1.5 mg MnO_2 were used instead of catalyst (all other components the same: [H_2O_2] = 125 mM, [Et_3N] = 50 mM, 5 mL MeOH), the initial rate of H_2O_2 decomposition was 0.3 mM/min, and only 19% of H_2O_2 was decomposed in 2 h.

2.5. Calculations

Geometry optimizations were performed using the program SIESTA [15] within the DFT framework using the Perdew–Burke–Ernzerhof exchange – correlation functional [16]. For all atoms, basis sets of double- ζ plus polarization quality were employed, with a pseudoatomic orbital energy shift of 25 meV and a grid cutoff of 150 Ry [15]. This combination of functional, basis sets, and grid parameters was validated previously [17]. Starting geometry was built in-silico from the structure of $Mn_2[(FHXTA)(H_2O)_4]^-$ (where H_5F-HXTA = 5-fluoro-2-hydroxy-1,3-xylene-α,α′-diamine-*N*,*N*,*N*′,*N*′-tetraacetic acid) [18]. Atomic coordinates are given in Table S1.

3. Results and discussion

3.1. Synthesis and spectroscopic characterization

Complex $Na[Mn^{III}_2L(OH)_2(H_2O)_2]\cdot 5H_2O$ (**1**·$5H_2O$) was synthesized by treatment of a solution of Na_4HL in a 94:6 MeOH:H_2O mixture, with five equiv. of triethylamine and two equiv. of $Mn(ClO_4)_2$. Complexation occurs immediately after mixing the Mn^{II} salt with the deprotonated ligand, as evidenced by the change of color of the reaction mixture from yellow to brown. Addition of base facilitates formation of Mn^{III} and deprotonation of the ligand for coordination to the metal. The solid complex is air stable, EPR silent and has a room temperature magnetic moment of 6.85 BM, which is slightly lower than 6.93 BM, corresponding to the spin-only value for two non-interacting high-spin Mn^{III} centers, with S1 = S2 = 2 and g = 2.0. When lowering the temperature, the $\chi_M T$ product continuously decreases from 5.87 $cm^3\,K\,mol^{-1}$ at 300 K to 1.92 $cm^3\,K\,mol^{-1}$ at 2 K suggesting an antiferromagnetic exchange between the Mn^{III} centers (Fig. 1). The magnetic behavior of the compound was analyzed using the isotropic spin Hamiltonian $H = -2J S_1S_2$ ($S_1 = S_2 = 2$) and the Van Vleck equation in the temperature range from 300 to 50 K [19]. In this temperature range, the least-squares fitting of experimental data gives $J = -2.5\ cm^{-1}$, and g = 2.02. The exchange splitting J value of **1** falls in the same range as other phenoxo-bridged Mn^{III}_2 compounds [20], which are characterized by weak magnetic coupling, and is smaller than the value of $-8.5\ cm^{-1}$ reported for a triply bridged Mn^{III}_2 complex with the (μ-phenoxo)bis(μ-acetato) core [21].

At low temperature, the simulated curve deviates strongly from the experimental data. The formation of chains [22], intermolecular interactions and zero-field splitting might cause this anomalous magnetic behavior [23]. The lack of crystal structure (several attempts to crystallize **1** failed) disabled a more detailed analysis of the magnetic data.

The thermogravimetric analysis indicates that two of the solvent molecules are coordinated to the metal centers of the complex. The broad band centered at 3425 cm^{-1} with a shoulder at 3270 cm^{-1} in the IR spectrum of the complex might account for the presence of two different types of water molecules in the solid (Fig. S1). The IR spectrum also shows intense bands at 1602/1405 cm^{-1} that can be attributed to the carboxylate groups of the ligand, the splitting of which suggests monodentate CO_2^- binding to Mn. The band at 1480 cm^{-1} belongs to the aromatic moiety while medium bands at 1323 and 1262 cm^{-1} may be attributed to C—N and C—O stretches of the ligand.

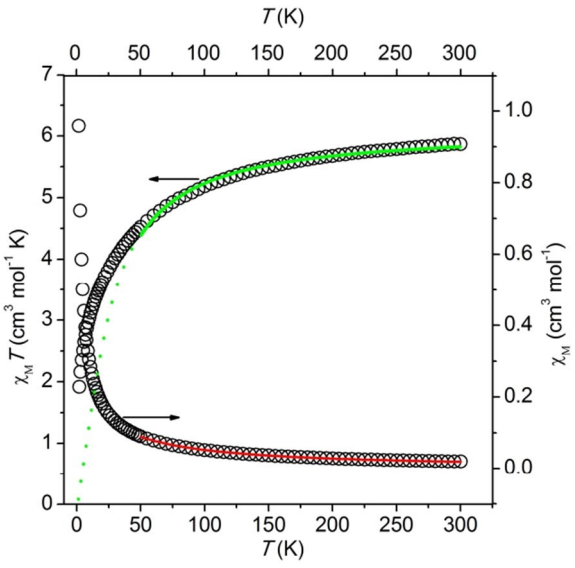

Fig. 1. Temperature dependence of $\chi_M T$ and χ_M for compound **1**. (O) experimental data, solid and dotted lines show the simulation obtained with the isotropic Hamiltonian (solid: fitting in the range 300–50 K; dots: simulation in the full T range).

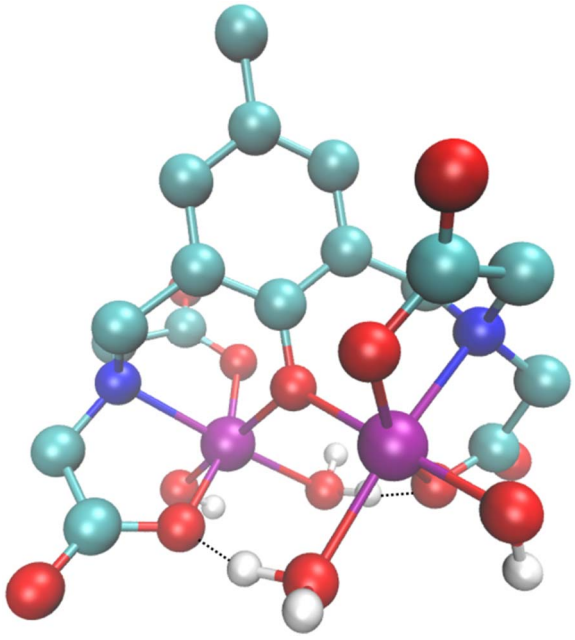

Fig. 2. Optimized geometry for the complex **1**. Carbon atoms are shown in green, nitrogen atoms are shown in blue, manganese atoms are shown in purple, and oxygen atoms are shown in red (the hydrogen atoms are not shown for clarity, except for the solvent molecules).

An optimized geometry for complex **1** is shown in Fig. 2, and calculated bond distances, atoms numbering and atomic coordinates are detailed in Fig. S2 and Table S1. In this structure, the two Mn ions are bridged by the central phenoxo group of the ligand and each metal ion is placed in a distorted hexacoordinate environment defined by a NO_3 donor set from L^{5-}, one hydroxo anion and one water molecule. The coordination polyhedra around the Mn ions may be described as elongated octahedral, with the axial H_2O—Mn—N bond distances (Mn-N/O_{av} 2.25 Å) distinctly longer than the equatorial Mn—O bond distances (Mn-O_{av} 1.97 Å), a signature of Jahn-Teller distorted Mn^{III} ions [24,25].

Even though the ligand is symmetric, the two Mn ions are not equivalent (in agreement with NMR studies described below). The H_2O-Mn-N elongation axes are twisted by 61.3° and the dihedral angle between the two Mn equatorial planes equals 80.0°. The calculated Mn···Mn distance of 3.67 Å and the Mn-O-Mn bridging angle of 126.4° can account for the small measured antiferromagnetic exchange constant (with antiferromagnetic contributions just prevailing over ferromagnetic ones).

Complex **1** is slightly soluble in water so most studies were performed in methanol. The molar conductivity for this compound in methanol is 96 $\Omega^{-1}\,cm^2\,mol^{-1}$, as expected for a complex that behaves as 1:1 electrolyte in solution [26]. ESI-mass spectra of complex confirm its chemical composition and retention of nuclearity in solution. The negative mode ESI-mass spectrum of a freshly prepared solution of the complex in MeOH shows two main peaks at m/z 534 and m/z 503 belonging to $[Mn_2L(OMe)]^-$ and $[Mn_2L]^-$ (Fig. 3(a), black line), respectively. Two other peaks detected at m/z 520 and 557 can be assigned to the dinuclear species $[Mn_2L(OH)]^-$ and $[Mn_2L(H_2O)_3]^-$, respectively. A similar spectrum is obtained 24 h after preparation of solutions of the complex in MeOH (Fig. 3(a), red line), showing the stability of the dinuclear complex in a 24-hour period.

The electronic spectrum of a methanol solution of complex **1** (Fig. 2(b), black line) exhibits two absorptions at 239 and 283 nm, assigned to π-π* transitions within the ligand. Moderately intense bands appear as a broad shoulder in the region 300–500 nm, and can be attributed to ligand-to-metal charge transfer (LMCT) transitions from pπ

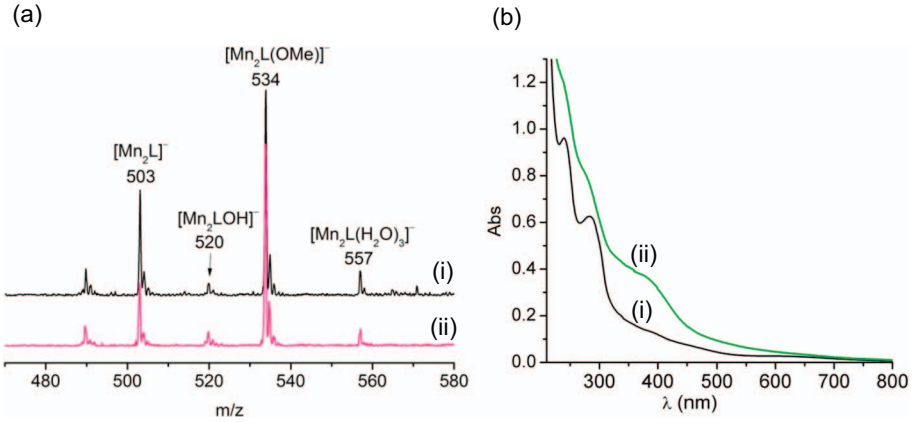

Fig. 3. (a) ESI-MS spectra of a MeOH solution of **1** immediately after preparation (i) and after 24 h (ii). (b) Electronic spectra of (i) 0.1 mM **1** and (ii) 0.07 mM **1** + 10 eq. Et_3N, in methanol.

orbital of phenolate to partially filled Mn^{III} d-orbitals [27,28], with some contribution of carboxylate-to-Mn^{III} CT [29]. The low intensity broad band at 602 nm corresponds to d-d transitions. In agreement with MS results, electronic spectra of the complex registered at different times after preparing the solutions, showed identical λ_{max} and molar absorbance coefficients, indicating that the complex is stable in methanol. Upon addition of Et_3N to a solution of **1** in methanol, π-π* transitions show slight blue-shift and higher intensity (Fig. 3(b), green line). The cyclic voltamogramm of **1** (Fig. S3) shows an irreversible reduction peak at Ep = 64 mV vs. Ag/AgCl attributed to the Mn^{III}/Mn^{II} couple.

^{1}H NMR spectroscopy was used as a way to determine the metal binding to donor sites of the ligand by analyzing the effect of addition of increasing amounts of $MnCl_2$ on the proton resonances of the ligand in D_2O. Upon addition of 0.1 to 0.5 equiv. of $MnCl_2$ to the D_2O solution of ligand significant changes were observed (Fig. 4). Resonances ascribed to both Ar–C$\underline{H}_2$-N (δ 3.77 ppm) and N-C$\underline{H}_2$-CO_2 (δ 3.23 ppm) show large broadening and the signal at 3.77 ppm is no longer observed in the diamagnetic region after addition of 0.3 equiv. of salt. The resonances of the aromatic protons and the 5-methyl group also show broadening and chemical shift displacement from the values observed for the free ligand. For the 1:1 metal to ligand mixture, spectral features of the ligand were no longer observed in the diamagnetic region. These data support the metal complexation through both the phenolate and carboxylate groups of the ligand.

The 1–10 ppm region of the ^{1}H NMR spectrum of **1** in D_3COD shows peaks belonging to the solvent without traces of the ligand, indicating

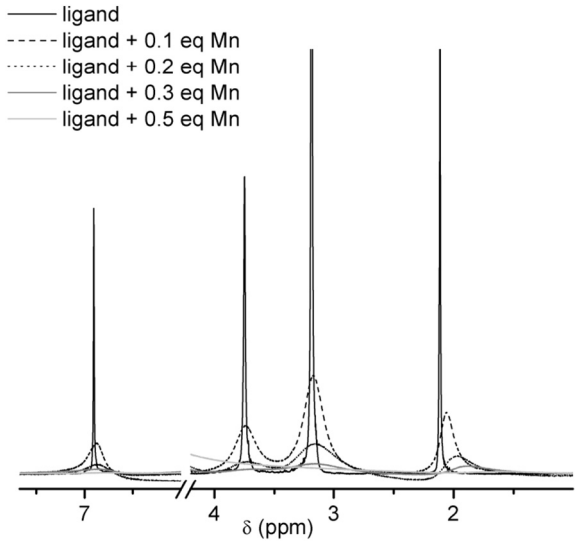

Fig. 4. ^{1}H NMR spectra of ligand + increasing amounts of $MnCl_2$ in D_2O.

the complex is stable towards metal dissociation in this solvent. The paramagnetic ^{1}H NMR spectrum of **1** in CD_3OD shows signals with isotropic shifts ranging from +40 to −25 ppm (Fig. S4). The observed isotropic shifts are consistent with the weak antiferromagnetic coupling of the two Mn^{III} ions in the complex [30]. The three more intense resonances at 8, 15 and 27 ppm, can be attributed to the methyl and phenolato ring protons shifted downfield as a consequence of spin-delocalization. These signals appear at δ values lower than observed for phenolato-bridged Mn^{III} dimers with long Mn···Mn separation and negligible magnetic exchange interactions [31]. Aromatic protons are not equivalent, indicating that the ligand is not symmetrically disposed around the two metal ions. Additionally, the broader peaks of methylene protons span the full range of the spectrum [32].

3.2. CAT activity

3.2.1. Kinetic and spectroscopic studies

The ability of **1** to catalyze disproportionation of H_2O_2 into O_2 and H_2O was tested in methanol by volumetric measurement of evolved O_2. Addition of H_2O_2 to a solution of the catalyst causes an immediate vigorous evolution of O_2 coupled to color change from dark brown to pale brown. When > 600 equivalents of H_2O_2 over complex were added, the solution turned yellowish-brown. The O_2 evolution was evaluated in excess of H_2O_2 and at constant temperature, and the dependence of the reaction rate with [catalyst] and [H_2O_2] was determined by varying [catalyst] at fixed [H_2O_2] (Fig. S5), and varying the [H_2O_2] at constant [catalyst] (Fig. S6).

At constant $[H_2O_2]_0$ = 155 mM, the reaction exhibits first-order kinetics on [catalyst], and the first-order rate constant k_1 = 49(2) min^{-1} was obtained from the slope of the plot of r_i vs. $[\mathbf{1}]_0$ (Fig. 5(a)). At fixed [catalyst] = 0.5 mM, initial rates show a good linear dependence with $[H_2O_2]_0$ (Fig. 5(b)) affording first-order rate constant k_1' = 0.147(2) min^{-1}. The second-order catalytic constant k_{cat} = 305(9) M^{-1} min^{-1} was obtained from either $k_1/[H_2O_2]_0$ or $k_1'/[cat]_0$.

The initial rate of O_2 evolution was also measured at 10 °C. At this temperature, the H_2O_2 disproportionation catalyzed by **1** retains the kinetic profile, but slows down (Fig. S7), affording k_{cat} = 79 M^{-1} min^{-1}. From rate constants at 10 and 25 °C, activation energy E_a = 61 kJ/mol could be estimated. This E_a is higher than the value of 35 kJ/mol reported for the H_2O_2 disproportionation by a related phenoxo-bridged di$Mn^{II,III}$ complex, in MeCN, which reacts faster than **1** [33] (see Section 3.2.2). In methanol, the complex converts > 600 equiv. of H_2O_2 to O_2 and H_2O. However, although successive additions of excess H_2O_2 to the catalyst solution yield the stoichiometric amount of O_2, the initial rate of H_2O_2 dismutation gradually decreases after each new addition (Fig. 6). UV–vis spectra taken on a 150:1 H_2O_2:**1** mixture show that the starting spectral pattern of the complex is retained, but the intensity of the absorption bands decreases

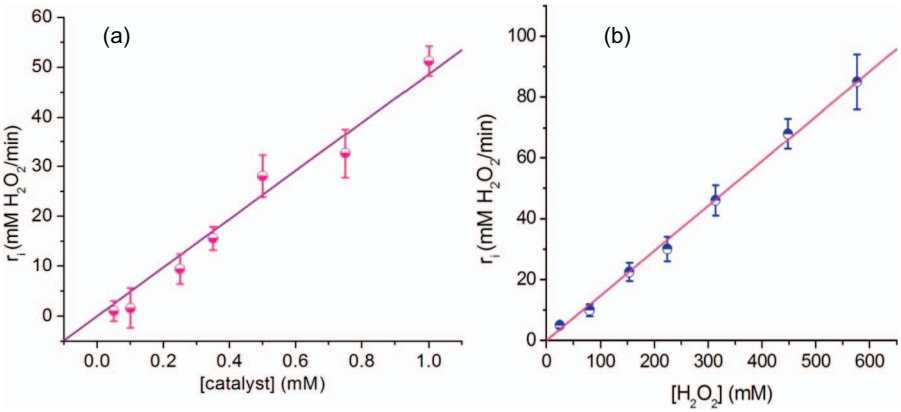

Fig. 5. Dependence of r_i on (a) [catalyst], at fixed $[H_2O_2]$ = 155 mM; and on (b) $[H_2O_2]$ at fixed [catalyst] = 0.5 mM, in MeOH. T = 25 °C.

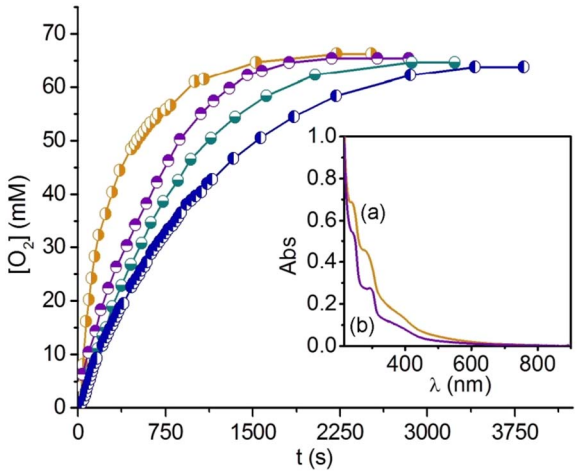

Fig. 6. Successive additions of 130 mM H_2O_2 on a methanol solution of 0.86 mM **1**. Inset: Electronic spectra of the catalyst before (a) and after (b) addition of 150 equiv. of H_2O_2 on a 0.07 mM **1** in MeOH. T = 25 °C.

immediately after H_2O_2 addition (Fig. 6, inset). At the end of the H_2O_2 disproportionation reaction, the intensity of starting spectrum is not completely recovered, probably as the consequence of partial metal dissociation (see below).

The 9 GHz band EPR spectrum of a frozen solution of **1** in methanol is shown in Fig. 7(a). This spectrum is essentially silent in line with a Mn^{III} based complex. After addition of 100 equiv. of H_2O_2 to a solution of **1** in methanol, the EPR spectra exhibited spin transitions extending over 0 to 7000 G (Fig. 7(b)). These features are characteristic of weakly coupled Mn^{II}_2 complexes [28,34–36] and originate from the contribution of the five populated paramagnetic S spin states (S = 1–5) [37]. Although poorly resolved, several sets of low intensity hyperfine lines could be detected on some signals, with an average spacing of ≈40–45 G (inset in Fig. 7(b)) typical of the interaction between the electronic spin and two Mn^{II} nuclear spins (I_{Mn} = 5/2). Superimposed to this broad spectrum, a six-line signal appears at $g \approx 2$ (hyperfine splitting of ≈90 G), with weak doublets inserted between the six absorptions (Δm = 1 nuclear-spin–forbidden transitions characteristic of the hyperfine structure of an uncoupled Mn^{II} ion). The spectral features of the coupled Mn^{II}_2 species were observed during the reaction course and disappeared once all H_2O_2 had been consumed, while the uncoupled Mn^{II} species persisted at the end of the reaction (Fig. 7(c)). These observations suggest that the Mn^{II}_2 species behaves as an active reduced form of the catalyst while the uncoupled Mn^{II} species accumulates as an inactive final product. This is in accordance with the gradual decrease of the bands intensity in the electronic spectra and in ESI-MS experiments during the reaction. This drop in intensity is the same as observed when lowering the solution pH. Addition of acid to the reaction mixture led to the loss of catalytic activity. Therefore, formation of an inactive uncoupled Mn^{II} species can arise from protonation of the bridging ligands and partial release of the metal.

Negative mode ESI-mass spectra recorded on a 100:1 H_2O_2:1 mixture during the reaction course, were dominated by the peak at m/z 503 that corresponds to Mn_2L^- along with peaks at m/z 543 and 557, corresponding to $[Mn_2L(OH)Na]^-$ and $[Mn_2L(H_2O)_3]^-$, respectively (Fig. 7(d)). Thus, the mass spectra confirm the involvement of the dinuclear complex in the catalytic cycle. Electronic spectroscopy, EPR

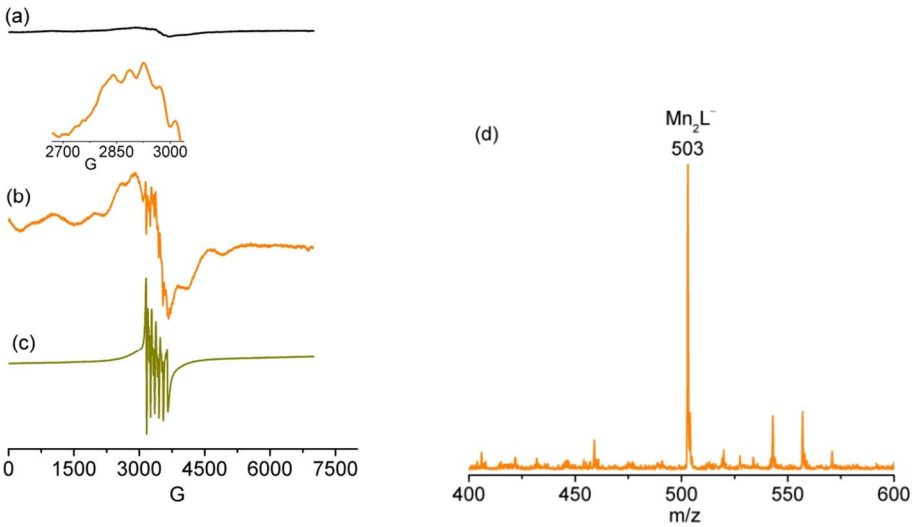

Fig. 7. X-band EPR spectra of (a) 1 mM **1** in methanol; (b) 1 mM **1** + 100 equiv. H_2O_2 a few minutes after mixing; (c) 1 mM **1** + 100 equiv. H_2O_2 at the end of the reaction. ν = 9.52 GHz, T = 120 K, microwave power = 0.5 mW. (d) ESI-mass spectrum of 1 mM **1** + 100 equiv. H_2O_2 taken during the reaction, negative mode.

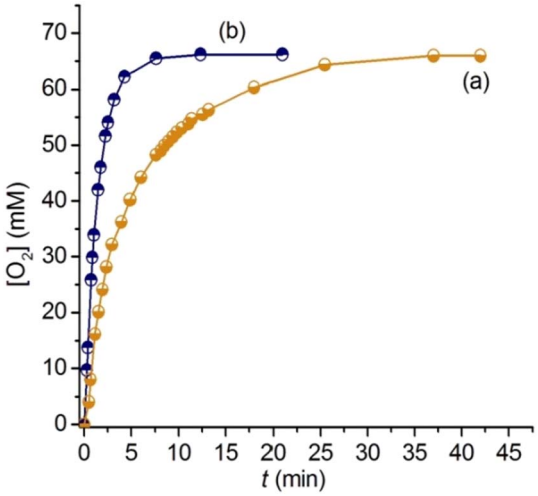

Fig. 8. O_2 evolution for the reaction of 0.86 mM cat + 130 mM H_2O_2 in (a) methanol and (b) 8.6 mM Et_3N in methanol. T = 25 °C.

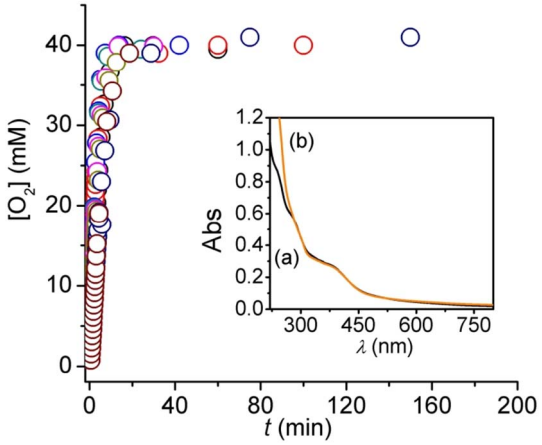

Fig. 9. Time-dependence of O_2 evolution after successive additions of 80 mM H_2O_2 to a solution of 0.55 mM **1** + 0.1 M Et_3N/Et_3NH^+ in methanol. Inset: Electronic spectra of the catalyst before (a) and after (b) addition of 150 equiv. of H_2O_2 on a solution of 0.05 mM **1** in basic MeOH. T = 25 °C.

and mass spectrometry results provide a clear indication that the starting complex alternates between dinuclear Mn_2^{II} and Mn_2^{III} species during the catalytic cycle, and that the lower rate of H_2O_2 decomposition observed after new additions of excess H_2O_2 results from partial dissociation of the metal.

In basic medium **1** is a better catalyst than in neat methanol (Fig. 8). The negative mode ESI-mass spectrum of **1** in basic methanol solution shows peaks at *m/z* 534 and 557, that can be attributed to $[Mn_2L(OMe)]^-$ and $[Mn_2L(H_2O)_3]^-$, respectively. These peaks also appear in the ESI-mass spectra taken after addition of 100 equiv. of H_2O_2 to the basic solution of **1** (Fig. S8), confirming the retention of the complex nuclearity during catalysis in this medium. But also in this case, after successive additions of 150 equiv. of H_2O_2 to a solution of **1** in Et_3N–MeOH, the rate of O_2 evolution decreases gradually as do the absorption bands in the electronic spectra of the complex after each new addition of H_2O_2. In this medium, no EPR signal due to a Mn_2^{II} species is observed during the reaction, and the intensity of the six-line signal of uncoupled Mn^{II} ion is lower than in neat methanol, indicating that the base slows down metal dissociation. The absence of an EPR signal during the reaction course, except for the final inactive Mn^{II} species, suggests that a Mn^{III} form of the catalyst is the dominant species in solution since no EPR signal is expected for the catalyst in this oxidation state. Thus, when the reaction is performed in Et_3N–MeOH, as base equivalents are consumed, ligand protonation results in metal dissociation with concurrent loss of activity, although in much lesser extent than in neat methanol.

The performance of the catalyst was improved by employing buffered solutions. When the reaction is performed in 50 mM Et_3N–Et_3NH^+, the catalyst retains its activity after successive additions of H_2O_2 with turnovers higher than 2000 (mol H_2O_2/mol catalyst). As shown in Fig. 9, the rate of O_2 evolution remains essentially constant after successive additions of 145 equiv. of H_2O_2, without significant changes in the electronic spectra (Inset of Fig. 9). Under these conditions, the reaction mixture is EPR silent, even at the end of the reaction. Besides, the rate of H_2O_2 disproportionation in buffered solution is the same as measured in the presence of 10 equiv. of Et_3N, suggesting that the exogenous base is not involved in catalysis but has the role of preventing protonation of the phenoxo-bridged diMn units.

The first order dependence of the reaction rate on the catalyst and the lack of time-lag at the onset of the reaction suggest that the starting Mn_2^{III} complex is the true catalyst. Based on spectroscopic results, the catalase activity of complex **1** in methanol involves a Mn_2^{III}/Mn_2^{II} cycle, where the reductive half-reaction (reduction of H_2O_2 to H_2O and concomitant oxidation of Mn_2^{II} to Mn_2^{III}) occurs in the slow step. Thus, the proportion of the reduced Mn_2^{II} form during catalysis is high enough to observe its characteristic broad EPR spectrum and a visible LMCT band of intensity lower than at the end of the reaction.

The catalytic cycle of H_2O_2 disproportionation by **1** can be explained as follow. In the starting complex, each Mn^{III} ion has a labile coordination site occupied by a solvent molecule (methanol or water), which facilitates terminal H_2O_2 binding through solvent/H_2O_2 exchange. Therefore, the catalytic cycle can initiate upon binding of peroxide to one of the Mn^{III} centers of the catalyst by displacement of a labile solvent molecule, followed by reduction of the Mn_2^{III} core to the Mn_2^{II} form (observed by EPR and ESI-MS) and release of O_2 (oxidative half-reaction) coupled to proton transfer, without change in the total formal charge of the catalyst. The carboxylate arms of the ligand can act as internal bases to assist the deprotonation of H_2O_2 [10]. In the reductive half-reaction, the substrate might bind the two Mn^{II} ions of the catalyst as a bridging $\mu_{1,1}$-peroxide, which upon protonation yields H_2O and restores the initial Mn_2^{III} complex, thus closing the cycle.

In the presence of base, the oxidized form of the catalyst is the major species during catalysis (no EPR signal is observed during catalysis). This suggests the oxidative half-reaction becomes the slow turnover limiting-step. Addition of 10 equiv. of Et_3N causes a threefold enhancement of initial rate. However, higher amounts of Et_3N do not cause any further significant increase, suggesting that the effect of the added base should be related to the stabilization of the catalyst, preventing the protonation of the ligand that leads to uncoupled inactive Mn^{II} species and demetallation.

3.2.2. Complex 1 compared to other MnCAT mimics

Catalytic dismutation of H_2O_2 usually shows saturation kinetics on substrate, described by the Michaelis–Menten model, where the initial rates (r_i) vs. $[H_2O_2]_0$ plots can be fitted to the equation: $r_i = k_{cat}$ [catalyst] $[H_2O_2]_0/(K_M + [H_2O_2]_0)$. In this equation, k_{cat} is the catalytic rate constant and K_M is a measure of the catalyst affinity for H_2O_2 (the lower the K_M value, the higher the affinity for H_2O_2). The fact that the initial rate does not achieve saturation with $[H_2O_2]$ may reflect a low affinity of **1** for the substrate (large K_M value). When $K_M \gg [H_2O_2]$, the denominator of the Michalis-Menten equation is dominated by K_M, and second-order kinetics is observed: $r_i = (k_{cat}/K_M)$ [catalyst] $[H_2O_2] = k$ [catalyst] $[H_2O_2]$. Therefore, the second-order rate constant can be taken as a measure of the catalytic efficiency of **1** and compared with k or k_{cat}/K_M of other studied catalysts. Table 1 lists k and k_{cat}/K_M values for complex **1** and diMn complexes with phenoxo bridged (Table 1, entries 2–7) and oxo-bridged diMn complexes with terminal carboxylato donors (Table 1, entries 8–9). The catalytic efficiency of **1** is in the range of other phenoxo-bridged diMn complexes obtained with

Table 1
Kinetic parameters for **1** and other dimanganese catalysts including polydentate ligands with a central bridging phenolate and/or terminal carboxylate groups.

	Complex	k or k_{cat}/K_M ($M^{-1}\,s^{-1}$)	Oxidation states during catalysis	Ligand donor set	Solvent	Refs
1	**1**	5.08	Mn_2^{II}/Mn_2^{III}	N_2O_5	MeOH	This work
2	$[Mn_2^{II,III}(bpbp)(\mu\text{-}OAc)_2]^{2+}$	3.76[a]	$Mn_2^{II,III}/Mn_2^{III,IV}$	N_6O	MeOH	[10]
3	$[Mn_2^{II,III}(bphpmp)(\mu\text{-}OAc)_2(H_2O)]^{+}$	4.36[a,b]	NR	N_5O_2	NR	[11]
4	$[Mn_2^{II,III}(bcpmp)(\mu\text{-}OAc)_2]$	11.44[a]	$Mn_2^{II,III}/Mn_2^{III,IV}$	N_4O_3	MeOH	[10]
5	$[Mn_2^{II,III}(bpbpmp)(\mu\text{-}OAc)_2(H_2O)]^{2+}$	14.5[b]	$Mn_2^{II,III}/Mn_2^{III,IV}$	N_5O	CH_3CN	[33]
6	$[Mn_2^{II}(bprol\text{-}^tBu\text{-}p)(\mu\text{-}OAc)(H_2O)_2]^{2+}$	0.29	NR	N_2O_3	DMF	[38]
7	$[Mn_2^{II,III}(bphba)_2(Cl)_2]$	1.1[a]	[c]	N_3O	H_2O	[40,41]
8	$[Mn_2^{III,IV}(\mu\text{-}O)_2(pda)_2]^{-}$	1.6	$Mn_2^{II,III}/Mn_2^{III,IV}$	N_2O_2	CH_3CN	[42]
9	$[Mn_2^{III,IV}(\mu\text{-}O)_2(bpg)_2]^{+}$	0.29	$Mn_2^{II,III}/Mn_2^{III,IV}$	N_3O	CH_3CN	[42]

NR = not reported. bcpmp = 2,6-bis({(carboxymethyl)[(1-pyridyl)methyl]amino}methyl)-4-methylphenol]; bpbp = 2,6-bis{[bis(2-pyridylmethyl)amino]methyl}-4-*tert*-butylphenol; Bpbpmp = 2-[bis(2-pyridylmethyl)aminomethyl]-6-{[(benzyl)(2-pyridylmethyl)amino]methyl}-4-methylphenol; bphba = 2-{(*N*,*N*-bis(2-pyridylmethyl)amino)methyl}phenol; bphpmp = 2-[bis(2-pyridylmethyl)aminomethyl]-6-{[(2-hydroxybenzyl)(2-pyridylmethyl)amino]methyl}-4-methylphenol; Hbpg = bis(2-picolyl)glycylamine; H3bprol-tBu-p = 2,6-bis(prolin-1-yl)methyl-4-*t*-butylphenol; H2pda = 2-picolyldiglycylamine.

[a] Saturation kinetics.

[b] Calculated from reported data.

[c] Mn_2^{III} form is the major species during reaction.

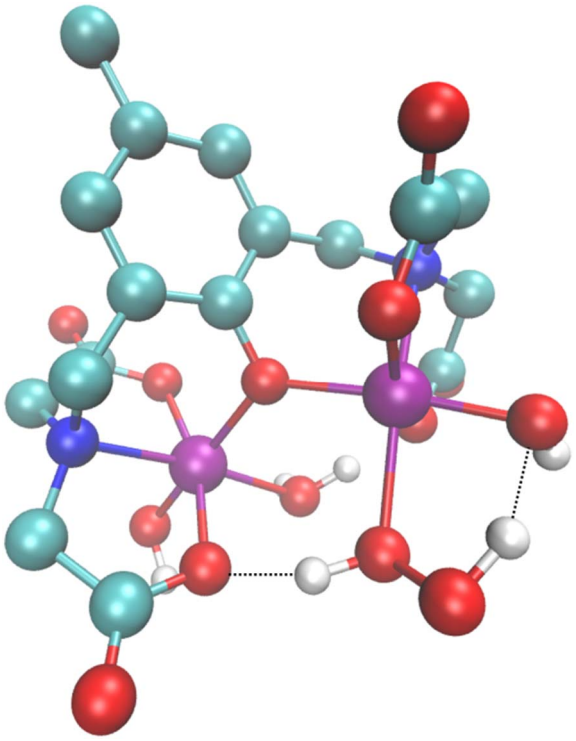

Fig. 10. Optimized geometry showing terminal carboxylate acting as internal base to assist deprotonation of H_2O_2. Calculated distances (Å): Mn-O_{peroxo} 2.27, H···$O_{hydroxo}$ 1.76 and H···$O_{carboxylate}$ 1.61. Carbon atoms are shown in green, nitrogen atoms are shown in blue, manganese atoms are shown in purple, and oxygen atoms are shown in red.

heptadentate ligands bearing either terminal tetrapyridyl [10], phenol/tripyridyl [11] or dipyridyl/dicarboxylato [10] donors (Table 1, entries 2–4), and with an hexadentate ligand possessing three terminal pyridyl donors and one non coordinating benzyl arm (Table 1, entry 5) [33]. These values are significantly higher than for the complex formed with a N_2O_3 pentadentate phenol-based ligand (entry 6 in Table 1) [38] - which reacts at a similar rate as other diMn complexes with pentadentate phenol-based ligands that have a N_4O donor set - [39], and are also better than for complexes possessing the $Mn_2(\mu\text{-}OPh)_2^{2+}$ core (Table 1, entry 7) [40,41].

It has been observed that for oxo-bridged diMn complexes of tripodal amine ligands (Table 1, entries 8–9) [42] and phenoxo-bridged diMn complexes of heptadentate ligands (Table 1, entries 2,4) [10], the pyridyl/carboxylato substitution increases the H_2O_2 disproportionation rate. For these complexes, the catalytic cycle involves $Mn_2^{II,III}$ and $Mn_2^{III,IV}$ oxidation states, with reduction of the $Mn_2^{III,IV}$ to the $Mn_2^{II,III}$ form occurring in the slow step (oxidative half-reaction). However, with four terminal carboxylato donors, **1** is half as efficient as the phenoxo-bridged diMn complex with terminal dipyridyl/dicarboxylato donors (bcpmp, entry 4 in Table 1). Since complex **1** cycles between Mn_2^{II} and Mn_2^{III} during catalysis and oxidation of the Mn_2^{II} form occurs in the slow step, the lower activity of **1** might result from the poor affinity of the Mn_2^{II} form of the catalyst for the substrate ($K_M \gg [H_2O_2]$), which should be even lower than observed for the oxidized $Mn_2^{III,IV}$ form of the complex with bcpmp (K_M = 3.17 M) [10]. Therefore, the low substrate affinity of the reduced form of **1** involved in the slow reaction step compensates the enhancement of catalytic activity caused by the increased number of terminal carboxylato groups (relative to complex with bcpmp).

4. Conclusions

The reaction of deprotonated L^{5-} with $Mn(ClO_4)_2$ in methanol-H_2O affords dinuclear $Na[Mn_2L(OH)_2(H_2O)_2]\cdot 5H_2O$ (**1**). The complex preserves the dinuclearity and keeps stable in solution for long time. ESI-mass spectrometry, electronic and EPR spectroscopy show that complex **1** catalyzes H_2O_2 disproportionation in methanol, with good efficiency and TON (mol of H_2O_2 disproportionated per mol of catalyst) > 600, by shuttling between homovalent Mn_2^{II}/Mn_2^{III} oxidation states. Based on electronic and EPR spectroscopy, the reduction of H_2O_2 is proposed to occur in the slow step of the catalytic cycle, just the same as observed for MnCAT from *L. plantarum* [43]. Protonation of the bridging and terminal ligands causes gradual loss of activity by metal dissociation, as the pH decreases. Demetallation is restrained upon addition of an exogenous base. Therefore, in buffered basic medium, TON > 2000 can be achieved without loss of activity. The involvement of Mn_2^{II} and Mn_2^{III} during catalysis distinguishes **1** from oxo-bridged diMn complexes of tripodal amine ligands [42] and other phenoxo-bridged diMn complexes with either heptadentate [10] or hexadentate [9,33] ligands that display catalase activity by redox cycling between $Mn_2^{II,III}$ and $Mn_2^{III,IV}$ oxidation states. Thus, having four carboxylate arms in such enclosing ligand does have several fallouts: (i) the four carboxylato groups of the ligand provide each Mn ion with an NO_3 environment that favors the formation of active homovalent diMn species, (ii) the negatively charged ligand precludes the formation of oxo-bridged species and, as a consequence, of high-valent Mn^{IV} ion(s) and (iii) the carboxylate arm due to its acid/base properties may impact the CAT activity by providing a potent internal base to assist deprotonation of H_2O_2, as shown in Fig. 10.

Acknowledgements

We thank the National University of Rosario (BIO401), CONICET (PIP 0337) and CNRS (PICS 263815) for financial support.

References

[1] S.V. Antonyuk, W.R. Melik-Adamiyan, V.R. Popov, V.S. Lamzin, P.D. Hempstead, P.M. Harrison, P.J. Artymiuk, V.V. Barynin, Crystallogr. Rep. 45 (2000) 105–116.
[2] V.V. Barynin, M.M. Whittaker, S.V. Antonyuk, V.S. Lamzin, P.M. Harrison, P.J. Artymiuk, J.W. Whittaker, Structure 9 (2001) 725–738.
[3] M.M. Whittaker, V.V. Barynin, T. Igarashi, J.W. Whittaker, Eur. J. Biochem. 270 (2003) 1102–1116.
[4] S. Signorella, C. Palopoli, V. Daier, G. Ledesma, R.H. Kretsinger, E.A. Permyakov, V.N. Uversky (Eds.), Encyclopedia of Metalloproteins, Springer, New York, 2013, pp. 1283–1292.
[5] P.J. Riggs-Gelasco, R. Mei, J.E. Penner-Hahn, H.H. Thorp, V.L. Pecoraro (Eds.), Mechanistic Bioinorganic Chemistry, American Chemical Society, Washington, DC, 1995(Chapter 8).
[6] S. Abdolahzadeh, J.W. de Boer, W.R. Browne, Eur. J. Inorg. Chem. (2015) 3432–3456.
[7] S. Signorella, C. Hureau, Coord. Chem. Rev. 256 (2012) 1229–1245.
[8] A.J. Wu, J.E. Penner-Hahn, V.L. Pecoraro, Chem. Rev. 104 (2004) 903–938.
[9] L. Dubois, R. Caspar, L. Jacquamet, P.-E. Petit, M.-F. Charlot, C. Baffert, M.-N. Collomb, A. Deronzier, J.-M. Latour, Inorg. Chem. 42 (2003) 4817–4827.
[10] R. Singh, M. Haukka, C.J. McKenzie, E. Nordlander, Eur. J. Inorg. Chem. (2015) 3485–3492.
[11] P. Karsten, A. Neves, A.J. Bertoluzzi, J. Strahle, C. Maichle-Mossmer, Inorg. Chem. Commun. 5 (2002) 434–438.
[12] G. Schwarzenbach, G. Anderegg, R. Sallmann, Helv. Chim. Acta 35 (1952) 1785–1792.
[13] M.E. Branum, A.K. Tipton, S. Zhu, L. Que Jr., J. Am. Chem. Soc. 123 (2001) 1898–1904.
[14] W. Chandler, E. Lee, D. Lee, J. Chem. Educ. 64 (1987) 878–881.
[15] J.M. Soler, E. Artacho, J.D. Gale, A. García, J. Junquera, P. Ordejón, D. Sánchez-Portal, J. Phys. Condens. Matter 2745 (2002) 2745–2779.
[16] J.P. Perdew, K. Burke, M. Ernzerhof, Phys. Rev. Lett. 77 (1996) 3865–3868.
[17] V. Demicheli, D.M. Moreno, G.E. Jara, A. Lima, S. Carballal, N. Ríos, C. Batthyany, G. Ferrer-Sueta, C. Quijano, D.A. Estrín, M.A. Martí, R. Radi, Biochemistry 55 (2016) 3403–3417.
[18] W.D. Kerber, J.T. Goheen, K.A. Perez, M.A. Siegler, Inorg. Chem. 55 (2016) 848–857.
[19] C.J. O'Connor, Prog. Inorg. Chem. 29 (1982) 203–283.
[20] G. Bhargavi, M.V. Rajasekharan, J.-P. Costes, J.-P. Tuchagues, Polyhedron 28 (2009) 1253–1260.
[21] R. Lomoth, P. Huang, J. Zheng, L. Sun, L. Hammarström, B. Åkermark, S. Styring, Eur. J. Inorg. Chem. (2002) 2965–2974.
[22] Y. Zhang, F.J. Huo, F. Gao, Acta Crystallogr. C C64 (2008) m67–m69.
[23] S. Sailaja, K. Rajender Reddy, M.V. Rajasekharan, C. Hureau, E. Rivière, J. Cano, J.-J. Girerd, Inorg. Chem. 42 (2003) 180–186.
[24] H. Biava, C. Palopoli, C. Duhayon, J.-P. Tuchagues, S. Signorella, Inorg. Chem. 48 (2009) 3205–3214.
[25] S. Mandal, A.K. Rout, M. Fleck, G. Pilet, J. Ribas, D. Bandyopadhyay, Inorg. Chim. Acta 363 (2010) 2250–2258.
[26] W.J. Geary, Coord. Chem. Rev. 7 (1991) 81–122.
[27] C. Hureau, L. Sabater, F. Gonnet, G. Blain, J. Sainton, E. Anxolabéhère-Mallart, Inorg. Chim. Acta 359 (2006) 339–345.
[28] L. Dubois, D.F. Xiang, X.S. Tan, J. Pécaut, P. Jones, S. Baudron, L. Le Pape, J.M. Latour, C. Baffert, S. Chardon-Noblat, M.N. Collomb, A. Deronzier, Inorg. Chem. 42 (2003) 750–760.
[29] M.M. Whittaker, C.A. Ekberg, R.A. Edwards, E.N. Baker, G.B. Jameson, J.W. Whittaker, J. Phys. Chem. B 102 (1998) 4668–4677.
[30] J. Bonadies, M.J. Maroney, V.L. Pecoraro, Inorg. Chem. 28 (1989) 2044–2051.
[31] M. Godziela, D. Tilotta, H.M. Goff, Inorg. Chem. 25 (1986) 2142–2146.
[32] D.W. Wright, H.J. Mok, C.E. Dubé, W.H. Armstrong, Inorg. Chem. 37 (1998) 3714–3718.
[33] L. Dubois, D.-F. Xiang, X.-S. Tan, J.-M. Latour, Eur. J. Inorg. Chem. (2005) 1565–1571.
[34] C. Hureau, L. Sabater, E. Anxolabéhère-Mallart, M. Nierlich, M.-F. Charlot, F. Gonnet, E. Rivière, G. Blondin, Chem. Eur. J. 10 (2004) 1998–2010.
[35] S. Blanchard, G. Blondin, E. Rivière, M. Nierlich, J.-J. Girerd, Inorg. Chem. 42 (2003) 4568–4578.
[36] C. Hureau, S. Blanchard, M. Nierlich, G. Blain, E. Rivière, J.-J. Girerd, E. Anxolabéhère-Mallart, G. Blondin, Inorg. Chem. 43 (2004) 4415–4426.
[37] S. Blanchard, G. Blain, Eric Rivière, M. Nierlich, G. Blondin, Chem. Eur. J. 9 (2003) 4260–4268.
[38] J. Kaizer, R. Csonka, G. Speier, React. Kinet. Catal. Lett. 94 (2008) 157–163.
[39] G. Eilers, C. Zettersten, L. Nyholm, L. Hammarstrom, R. Lomoth, Dalton Trans. (2005) 1033–1041.
[40] N. Reddig, D. Pursche, M. Kloskowski, C. Slinn, S.M. Baldeau, A. Rompel, Eur. J. Inorg. Chem. (2004) 879–887.
[41] S. Signorella, A. Rompel, K. Büldt-Karentzopoulos, B. Krebs, Vincent L. Pecoraro, J.-P. Tuchagues, Inorg. Chem. 46 (2007) 10864–10868.
[42] L. Dubois, J. Pécaut, M.-F. Charlot, C. Baffert, M.-N. Collomb, A. Deronzier, J.-M. Latour, Chem. Eur. J. 14 (2008) 3013–3025.
[43] M. Shank, V. Barynin, G. Dismukes, Biochemistry 33 (1994) 15433–15436.